THE ASTROPHYSICAL JOURNAL, 478:124–133, 1997 March 20

THE INTERMEDIATE-MASS STELLAR POPULATION OF THE LARGE MAGELLANIC CLOUD CLUSTER NGC 1818 AND THE UNIVERSALITY OF THE STELLAR INITIAL MASS FUNCTION[1]

DEIDRE A. HUNTER
Lowell Observatory, 1400 West Mars Hill Road, Flagstaff, AZ 86001

ROBERT M. LIGHT
IPAC, California Institute of Technology, 100-22, Pasadena, CA 91125

JON A. HOLTZMAN
Department of Astronomy, New Mexico State University, Las Cruces, NM 88003

ROGER LYNDS AND EARL J. O'NEIL, JR.
Kitt Peak National Observatory, National Optical Astronomy Observatories, P.O. Box 26732, Tucson, AZ 85726

AND

CARL J. GRILLMAIR
Jet Propulsion Laboratory, Mail Stop 183-900, California Institute of Technology, 4800 Oak Grove Drive, Pasadena, CA 91109

Received 1996 July 31; accepted 1996 October 5

ABSTRACT

We present stellar photometry from *Hubble Space Telescope* images of NGC 1818, a young populous star cluster in the Large Magellanic Cloud. The cluster stars in both the core and the outlying regions are well resolved, and the photometry extends to a V magnitude of 26, corresponding approximately to a K4 V star. With the use of isochrones, we compute a stellar initial mass function (IMF) for stars from 0.85 to 9 $M_{\odot}$. The slope of the mass function is -1.23 ± 0.08, which is close to the Salpeter (1955) slope of -1.35. The NGC 1818 star cluster represents a star forming event intermediate between that of open clusters and of globular clusters in terms of the mass of stars formed and their spatial concentration. The products of the star forming event itself, as a diagnostic of the physical processes, indicate that star formation in NGC 1818 proceeded in a manner similar to that in events that are both less and more concentrated or rich in stars. We compare IMF slopes that have been measured from star counts in clusters and associations in Local Group galaxies, and we conclude that for young stellar clusters and associations the IMF is independent of the spatial concentration of the stars formed, the richness of stars formed, galactic characteristics including metallicity, and, at least down to 0.85 $M_{\odot}$, the stellar mass range.

Subject headings: galaxies: star clusters — Magellanic Clouds — stars: luminosity function, mass function

1. INTRODUCTION

This study is the last in our series exploring the stellar initial mass function of intermediate-mass stars in young star clusters found in different galactic environments. Since the refurbishment of the *Hubble Space Telescope* (*HST*), the Wide Field and Planetary Camera (WFPC2) has enabled us to probe the stellar content of clusters to lower stellar masses in more crowded environments than is possible from ground-based telescopes. These studies have included the center of the luminous, compact cluster R136 in the Large Magellanic Cloud (LMC) (Campbell et al. 1992; Hunter et al. 1995, 1996c), the giant H II region NGC 604 in M33 (Hunter et al. 1996a), and the largest OB association in M31, NGC 206 (Hunter et al. 1996b). We have measured the stellar initial mass function in these clusters for intermediate-mass stars, where here the measured mass range varies from cluster to cluster but generally "intermediate" mass means less than 18 $M_{\odot}$. In this paper we extend our study to an example of a "populous" star cluster in the LMC, NGC 1818. Our objective is to determine whether the stellar initial mass function, as a diagnostic of the star formation process, varies among different galactic environments or different types of star forming events (that is, concentration and richness of stars formed).

NGC 1818 is one of the brightest and youngest among those star clusters in the LMC that are sometimes referred to as "blue globular clusters" or "populous clusters." Hodge (1961) made a plea for using the term populous cluster to refer to these objects since the term globular cluster implies a connection to Milky Way star clusters of that name that has not been shown to exist in all cases. Gascoigne & Kron (1952), for example, suggested that these clusters may be more like open clusters of unusually high luminosity and high concentration. NGC 1818 is not as luminous or as concentrated as R136 in the same galaxy, but rather it represents a less extreme and perhaps more common mode of star formation in the LMC. Still, the populous clusters appear as something of an anomaly compared to the star clusters most common in the Milky Way, being more rich and compact than a typical open cluster or association. It is interesting, therefore, to examine the nature of the star formation process through its stellar products in a star forming event that is intermediate between the extremes of cluster formation in the Local Group and to compare the characteristics of this cluster with those of other types of clusters and associations.

[1] Based on observations with the NASA/ESA *Hubble Space Telescope*, obtained at the Space Telescope Science Institute, which is operated by AURA, Inc., under NASA contract NAS 5-26555.

Brightnesses of individual stars have been measured before in NGC 1818 (Woolley 1960; Robertson 1974; Will, Bomans, & de Boer 1995). The cluster is known to contain blue and red supergiants, and the main sequence has been traced down to a V magnitude of 21.75 by Will et al. NGC 1818 is also known to be relatively young. Searle, Wilkinson, & Bagnuolo (1980) classed it as their type "I" (youngest category) cluster from integrated *uvgr* photometry, while van den Bergh (1981) classed it as "young" from *UBV* photometry. From photographically determined color-magnitude diagrams, Hodge (1983) assigned the cluster an age of 17 Myr, and Elson & Fall (1988) determined an age of 26 Myr. More recently, Will et al. (1995) used CCD photometry to deduce an age of 20 or 40 Myr, depending on the treatment of convective overshooting in the stellar evolution models used. Thus, NGC 1818 is a relatively young cluster, although not as young as the objects that we have examined previously in this series.

Here we discuss photometry of individual stars in NGC 1818 measured from WFPC2 images obtained with *HST*. The center of the cluster was placed on the PC1 CCD, and the outer parts of the cluster spilled over onto the WF CCDs. Due to the shape of the combined field of view, a northern segment of the cluster is not imaged. The scale of the WF CCDs at the LMC, where we assume a distance modulus of 18.5 (Panagia et al. 1991), is 0.024 pc per pixel, and the PC scale is approximately half this. The field of view is roughly 37 pc. Images taken through the F336W, F555W, and F814W (roughly *UVI*) filters allow us to plot color-magnitude and color-color diagrams. We have measured the main sequence to an F555W magnitude of 26 (corresponding roughly to a K4 V star) throughout the cluster including the core. After correcting statistically for background/foreground contamination, we determine an initial mass function (IMF) for the intermediate-mass stars from comparison with isochrones. Finally, with the evidence available to date for numerous clusters including NGC 1818, we address the question of the universality of the IMF in different galactic environments.

2. OBSERVATIONS AND DATA REDUCTION

The star cluster NGC 1818 was observed with the WFPC2 on *HST* on 1995 December 8. A comparison LMC background field was observed on 1995 July 6. The observations are listed in Table 1. Multiple short and long exposures through F336W, F555W, and F814W were obtained. A mosaic of the short F555W exposure of the cluster and an enlarged view of the PC image are shown in Figure 1 (Plates 2–3). The center of the cluster was placed on the PC CCD, letting the outer part of the cluster fall on the WF CCDs. The background field was chosen to be 9′ to the south of the cluster, in a region of the LMC deemed free of stellar clusters or associations as seen on the atlas compiled by Hodge (1967). By remaining relatively close to the cluster itself, however, we are sampling a stellar population of the LMC and Milky Way likely to be similar in stellar density to that in front of or behind NGC 1818. In even the short exposures of the cluster, the brighter cluster stars are saturated; our focus here is on the intermediate and lower mass stars.

The different images for the same filter and exposure were averaged with an algorithm to remove cosmic rays by identifying pixels that deviated from the average. Shifting the images before adding them was found to be unnecessary.

Stellar photometry was performed using the crowded-star photometry package DAOPHOT (Stetson 1987) as implemented in the Image Reduction and Analysis Facility (IRAF) software (Davis 1994). We experimented with a variety of fitting functions and fitting radii, but, as before, found that a simple Gaussian function worked best on both PC and WF images in the sense of always converging and leaving the smallest residuals. Erroneously detected objects in and around saturated stars and along their diffraction spikes were eliminated from the photometry files using a combination of cuts on the basis of sharpness and chi parameters returned by DAOPHOT, removing anything within a radius of 20–30 pixels from the centers of saturated stars, and by examining the images by eye. The photometry from the short exposures was combined with that from the long exposures for each filter. In cases where stars were measured on both the short and long exposures, the final photometry was a mean weighted by the uncertainties in the individual measurements. The uncertainty in the average magnitude is the dispersion around the mean.

The first five lines of the cluster photometry file are given in Table 2 and for the background field in Table 3. The stars are ordered by brightness in F555W, and the files in their entirety are available on the AAS CD-ROM Series, Vol. 7. A star had to be measured in F555W or F814W in order to be retained. The computed uncertainty in the final photometry is shown as a function of magnitude for the cluster stars in Figure 2. In this plot, for F555W and F814W one can see stars near the limit of the short exposure (high σ) that were not also detected on the longer exposures due, primarily, to their proximity to saturated stars. The observed color-magnitude diagrams are shown in Figures 3 and 4 for the cluster and background fields. The cluster color-color diagram is shown in Figure 5. No attempt was made to correct the F336W magnitudes for effects due to

TABLE 1

THE OBSERVATIONS

Object	Filter	Exposure (s)	Gain (e^-/DN)	Images
NGC 1818	F336W	160	7	u2pu0109t,u2pu010at,u2pu010bt, u2pu010ct,u2pu010dt,u2pu010et
	F555W	20	7	u2pu0101t,u2pu0102t
		140	7	u2pu0103t,u2pu0104t,u2pu0105t, u2pu0106t,u2pu0107t,u2pu0108t
	F814W	30	7	u2pu010ft,u2pu010gt,u2pu010ht
		200	7	u2pu010it,u2pu010jt,u2pu010kt, u2pu010lt,u2pu010mt,u2pu010nt
Background......	F336W	160	7	u2pu0209t,u2pu020at,u2pu020bt, u2pu020ct,u2pu020dt,u2pu020et
	F555W	20	7	u2pu0201t,u2pu0202t
		140	7	u2pu0203t,u2pu0204t,u2pu0205t, u2pu0206t,u2pu0207t,u2pu0208t
	F814W	30	7	u2pu020ft,u2pu020gt,u2pu020ht
		200	7	u2pu020it,u2pu020jt,u2pu020kt, u2pu020lt,u2pu020mt,u2pu020nt

TABLE 2

THE CLUSTER PHOTOMETRY[a]

Star	x[b]	y	F336W	σ	F555W	σ	F814W	σ	F336W–F555W	σ	F555W–F814W	σ
10001......	990.9	927.9	100.00	100.00	14.50	0.06	100.00	100.00	100.00	100.00	100.00	100.00
10002......	863.1	818.7	100.00	100.00	14.66	0.06	14.60	0.03	100.00	100.00	0.06	0.07
10003......	950.1	841.1	100.00	100.00	15.02	0.06	15.08	0.04	100.00	100.00	−0.06	0.07
10004......	960.1	978.4	100.00	100.00	15.06	0.05	15.10	0.02	100.00	100.00	−0.03	0.06
10005......	999.3	863.1	14.19	0.04	15.34	0.05	15.43	0.03	−1.15	0.07	−0.09	0.06
						. . .						

[a] The full text of this table, for all 11,921 stars, can be obtained on the AAS CD-ROM Series, Vol. 7.

[b] The x, y coordinates are those in the short-exposure F555W image, and the coordinate system is indicated in Fig. 1.

the red leak of the filter, which accounts for the anomalous blueward curvature at the faint end of the F336W–F555W versus F555W color-magnitude diagram. The F336W magnitudes are useful primarily for the blue stars.

Incompleteness fractions were determined through experiments in which we added artificial stars to the images, processed them in the same way as the original data, and counted the number of artificial stars, as a function of magnitude, that were recovered. Stars were added to each of the short and long exposure F555W and F814W images. The same stars that were added to the F555W images were added to the corresponding F814W image with the assumption of an F555W–F814W color of 0.5, an average of the range in colors found within the cluster. Artificial stars were added in numbers per magnitude bin equal to 10% of the luminosity function of the real cluster in order not to increase significantly the crowding in the image. In order then to build up statistics, we performed 200 experiments on each image. In the WF2 and WF4 CCDs, the crowding varied significantly over the images, so the field of view was divided up into a more crowded region, referred to as "Cluster," and a less crowded region, referred to as "Rest," and separate incompleteness fractions were determined for these two regions. The final incompleteness fraction is a combination of that for the short and that for the long exposures—a star only has to be detected on one of the exposures. We also required that stars be detected in either F555W or F814W. The percentages of stars lost as a function of magnitude are shown in Figure 6, and were applied as a correction factor in determining the IMF.

A comparison of the magnitude of the artificial star that was added to the images with the magnitude that was actually measured is an indication of the photometric uncertainties, perhaps a more reliable estimate than the more formal uncertainties. We have displayed this comparison for the long PC1 exposure, our worst case, in Figure 7, showing the error in measuring the F555W magnitude and the F555W–F814W color. Because the 48,000 points smear together, what one primarily sees in the figure is the outer envelope of the errors, which is consistent with the variation in computed σ with magnitude; that is, the error envelope is several σ.

3. REDDENING AND ISOCHRONES

There are several estimates of reddening for NGC 1818 in the literature, all from stellar photometry of only the brighter stars in the outer part of the cluster. Robertson (1974) concluded that $E(B-V)$ was 0.09 in NGC 1818, Cassatella et al. (1987) found $E(B-V)$ to be 0.07, Meurer, Cacciari, & Freeman (1990) measured a value of 0.05, and Will et al. (1995) determined a value of 0.07. Burstein & Heiles (1984) estimate the foreground contribution to $E(B-V)$ as 0.05. Here we adopted an $E(B-V)$ of 0.05 to begin with and found that no further adjustments were necessary. We used the *HST* flight filter extinction for a given $E(B-V)$ as tabulated by Holtzman et al. (1995), which is based on the reddening curve of Cardelli, Clayton, & Mathis (1989) and an R_V of 3.1. We averaged the tabulation for an O star and that for a K star since the stars in the cluster cover this range. The F336W, F555W, and F814W extinction corrections are 0.24, 0.16, and 0.10 mag, respectively. The color-color diagram in Figure 5 confirms that this low value of reddening is appropriate.

The isochrones are those of Holtzman et al. (1995). They are based on the stellar evolution models for LMC-like metallicity of Schaerer et al. (1993) and have been transformed to the WFPC2 filter system using Kurucz (1993) model atmospheres and filter and system response functions. In applying these isochrones to the LMC cluster

TABLE 3

THE BACKGROUND FIELD PHOTOMETRY[a]

Star	x[b]	y	F336W	σ	F555W	σ	F814W	σ	F336W–F555W	σ	F555W–F814W	σ
10001......	865.5	976.7	19.68	0.05	17.46	0.02	16.25	0.01	2.21	0.05	1.21	0.02
10002......	1072.9	849.8	21.02	0.07	18.77	0.04	17.55	0.01	2.25	0.08	1.22	0.04
10003......	856.6	855.9	18.33	0.01	19.02	0.05	19.06	0.03	−0.69	0.05	−0.04	0.05
10004......	946.2	1096.7	20.00	0.06	19.45	0.05	18.94	0.03	0.56	0.08	0.50	0.06
10005......	1094.7	915.8	100.00	100.00	19.58	0.04	19.60	0.03	100.00	100.00	−0.02	0.05
						. . .						

[a] The full text of this table, for all 7021 stars, can be obtained on the AAS CD-ROM Series, Vol. 7.

[b] The x, y coordinates are those in the long-exposure F555W image.

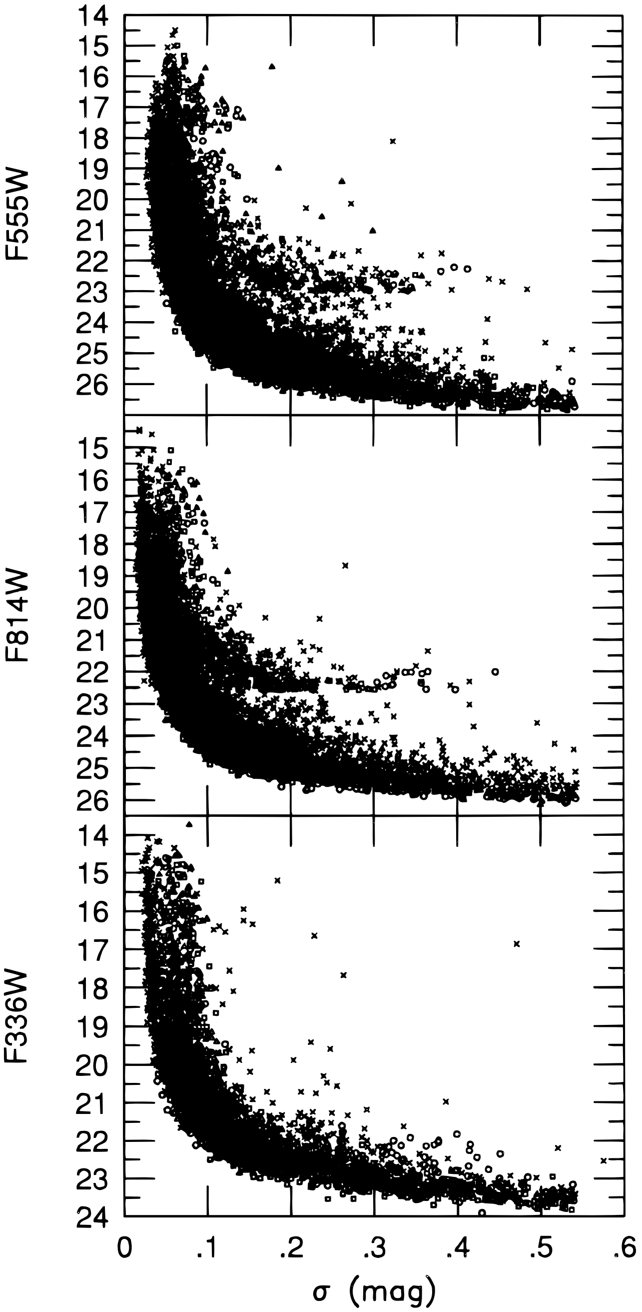

FIG. 2.—Computed photometric uncertainty in each filter is shown as a function of magnitude. The different symbols distinguish the different CCDs: PC1 is denoted by crosses, WF2 by open triangles, WF3 by open circles, and WF4 by open squares. The combined photometry (short and long exposures) is shown and sigmas of stars observed in both exposures is the dispersion around the mean. The dual branch at higher σ is due to stars near the limit of the short exposure (high σ) that were not also detected on the longer exposures due, primarily, to their proximity to saturated stars.

R136, Hunter et al. (1995) had found it necessary to apply a correction to the isochrones for reasonable fits to the data, and added 0.06 to F555W–F814W and 0.07 to F336W–F555W. Hunter et al. assumed that this discrepancy was due to errors in the zero points, especially for F336W; and they discussed sources of uncertainty. Using the same corrected isochrones here, we find that the isochrones lie along the ridgeline of the data for the unevolved, main-sequence portion of the color-magnitude diagram in F555W–F814W versus F555W. However, the isochrones are too blue in F336W–F555W by 0.2 mag. We have had this problem with F336W–F555W and the isochrones for other objects covering a range in metallicities (NGC 206, Hunter et al. 1996b; IZw18, Hunter & Thronson 1995), and metallicity is a possible contributor. The metallicity of the NGC 1818 cluster is known to be about $Z \sim 0.003$ from spectroscopy of two supergiant stars (see analysis in Will et al. 1995), while the isochrones are for $Z = 0.008$. Thus, the cluster is somewhat more metal poor than the isochrones. However, the offset in the isochrones is counter to what one expects for effects due to metallicity, and difficulties with calibrating the F336W filter are possible. We have, as before, opted to fudge the F336W–F555W isochrones, adding an additional 0.2 mag to the color. The colors of the isochrones are used to examine the age and evolutionary state of the stars in the cluster; the mass assignments themselves depend only on the F555W magnitudes of the stars.

4. BACKGROUND SUBTRACTION, COLOR-MAGNITUDE DIAGRAMS, AND AGES

We have used the background field, located 9′ south of the cluster, to statistically subtract foreground Milky Way and background LMC stars in the field of view of the cluster. Brightnesses of stars in the background field were measured in the same way as for the cluster itself. Separate incompleteness corrections were found for the background field since the absence of the more luminous stars found in the cluster would be expected to alter the incompletenesses. The background stars were binned in 0.5 mag and 0.5 F555W–F814W color bins; separate count was made of stars found only in F555W or in F814W. The counts were multiplied by the ratio of the incompleteness factor in the background to that in the cluster. The four CCDs were averaged together, with normalization by area, to increase the statistics. Stars in each magnitude and color bin were deleted randomly from the cluster photometry lists according to these background counts, scaled by the area of the particular CCD or region of the CCD.

The color-magnitude diagrams of the cluster after this statistical background correction has been applied are shown in Figure 8. One can see that there are a few stars in the cluster color-magnitude diagrams that are on the red giant branch (F555W–F814W ~ 1; $M_{\mathrm{F555W},0} \sim 0.5$) and are residual field stars. Background subtraction is not perfect most likely because of small number statistics. These red giant stars are eliminated in constructing the IMF.

The color-magnitude diagrams show a well-developed main sequence down to an $M_{\mathrm{F555W},0}$ of about 7, which corresponds to a star of approximately 0.74 $M_{\odot}$ according to the isochrones. There are also brighter stars in the cluster center that do not appear on these color-magnitude diagrams because they are saturated in our images. About two dozen stars are saturated on our short exposures, and these are red and blue supergiants according to Will et al. (1995).

From ground-based BV photometry, Will et al. (1995) concluded that NGC 1818 was 20 or 40 Myr old depending on the treatment of convective core overshoot in the isochrones they used. Models including convective core overshoot gave the older age. Relative to the isochrones that we are using, the younger age is indicated. By 20 Myr, stars brighter than an $M_{\mathrm{F555W},0}$ of -3.1 should have evolved off the main sequence according to the Schaerer et al. (1993) models. By 40 Myr, the top of the isochrone has dropped to about -2.3. Yet, we see stars on or near the main sequence

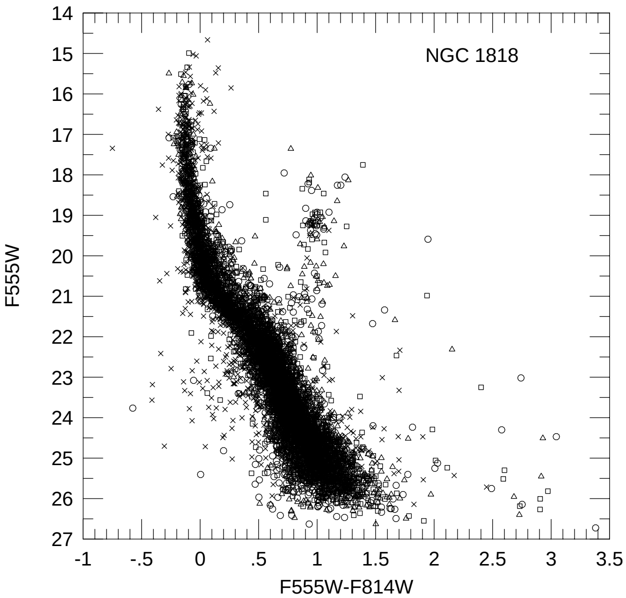

FIG. 3a

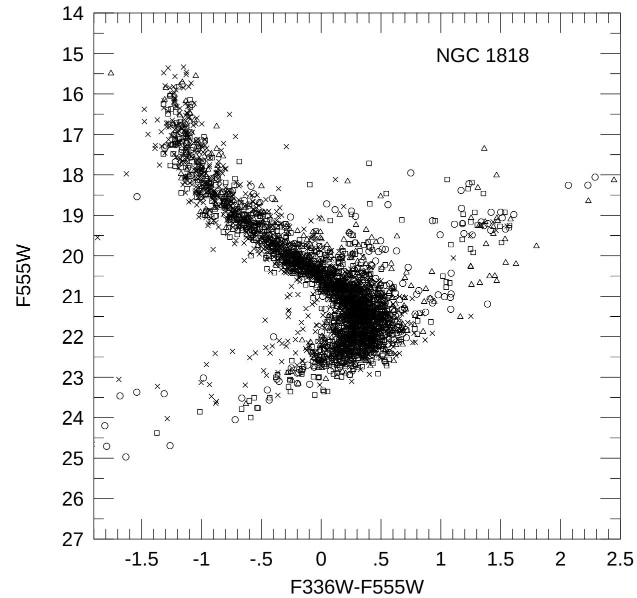

FIG. 3b

FIG. 3.—Observed color-magnitude diagrams for the cluster. (*a*) F555W–F814W and (*b*) F336W–F555W. The different symbols denote the different CCD chips: *crosses*, PC1 photometry; *open triangles*, WF2; *open circles*, WF3; *open squares*, WF4. No attempt was made to correct the F336W magnitudes for effects due to the red leak of the filter, which accounts for the anomalous blueward curvature at the faint end of the F336W–F555W versus F555W color-magnitude diagram.

in NGC 1818 up to nearly -3.5. Thus, an age like 20 Myr is indicated by the top of the color-magnitude diagram for the Holtzman et al. (1995) isochrones we used.

At the fainter end, however, the story is potentially different. One can see that the isochrones for 10 and 20 Myr arc redward in $(\mathrm{F555W{-}F814W})_0$ around an $M_{\mathrm{F555W},0}$ of 5.5 as a result of stars still on pre–main-sequence tracks. According to Stahler (1983) a star of 0.8 $M_{\odot}$ (about an $M_{\mathrm{F555W},0}$ of 6.4) should be near, but not on, the zero-age main sequence by 20 Myr. However, by 30 or 40 Myr these stars have moved closer to the zero-age main sequence, and the isochrones straighten blueward as can be seen in Figure 8. These older isochrones, more than 30 Myr, seem to trace the ridgeline of the faint stars better than the younger isochrones do. Thus, at face value it would seem that the less massive stars indicate an older age than the massive stars, and that the cluster has formed stars over a period of time. This has long been the standard view of how star formation proceeds in a cluster, although evidence of counterexamples is also seen (see, e.g., Hillenbrand et al. 1993; Hunter et al. 1995). However, a cautionary note is in order. We are

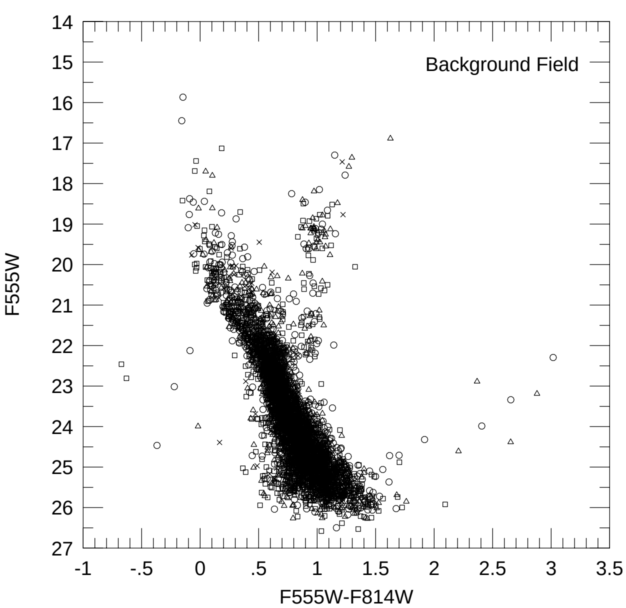

FIG. 4.—Color-magnitude diagram for stars in the background field. The different symbols identify photometry from the different CCD chips and are the same as in Fig. 3.

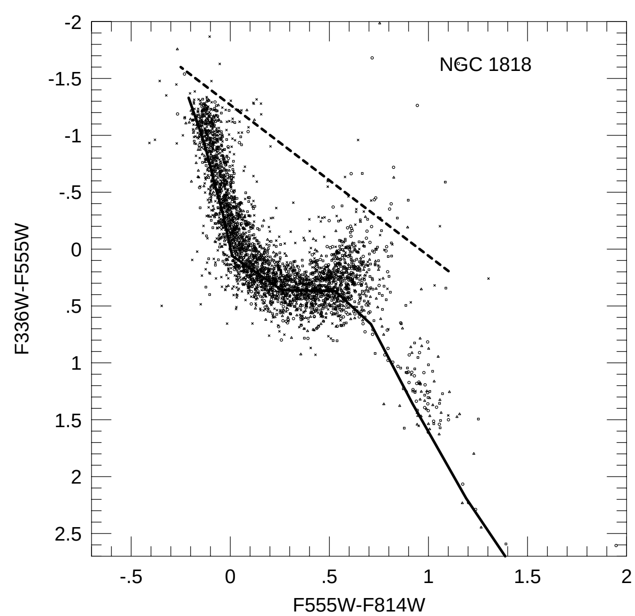

FIG. 5.—Observed color-color diagram for cluster stars measured in all three filters is shown. The solid line is a 20 Myr isochrone and, the dashed line is the reddening vector for an $E(B-V) = 1$. The individual points are made tiny in order to make the isochrone more visible.

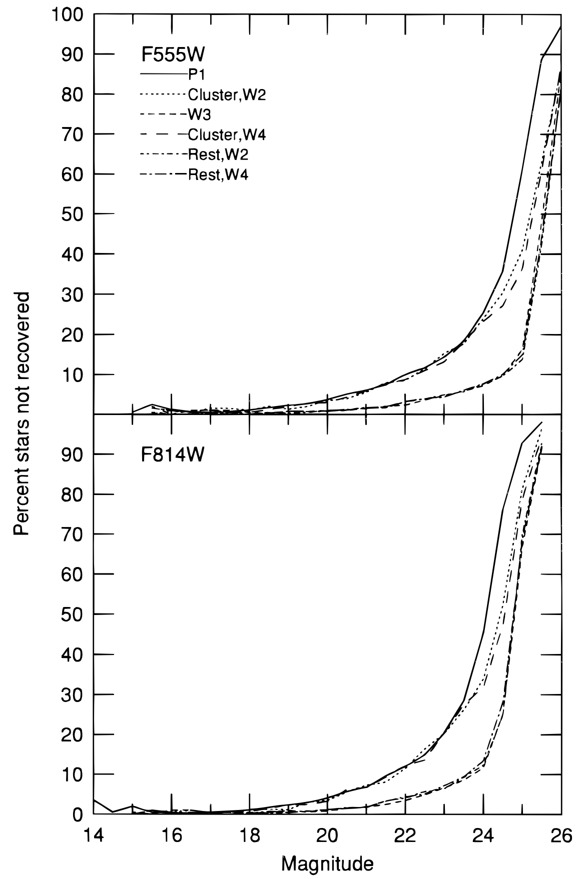

FIG. 6.—Incompleteness in terms of percentage of fake stars that were added to the images and not recovered. There is a different incompleteness for the more crowded regions of the WF2 and WF4 images ("Cluster") and for the less crowded regions ("Rest"). F555W and F814W were treated separately.

talking about the faint end of the photometry where photometric uncertainties in F555W–F814W are of order several tenths, while the difference between the 20 Myr isochrone and the 30 Myr isochrone is only of order 0.07 in the color. Thus, the lower age limit for the lower mass stars in the cluster is highly uncertain.

Since we have to select an isochrone to use in assigning masses based on the $M_{F555W,0}$ and because the younger isochrone is consistent with the presence of the more luminous stars, we have chosen to use 20 Myr as the age of the cluster. We did, however, explore the consequence to the IMF of using an older isochrone. In this case the top mass bin drops out and the IMF slope flattens by 1 σ. Thus, the choice of specific isochrone does not affect the results significantly.

5. STELLAR INITIAL MASS FUNCTION

In compiling the counts of stars in different mass bins, we have applied the incompleteness corrections shown in Figure 6. In addition we corrected for the missing piece of the cluster due to the shape of the field of view of the WFPC2. The cluster center was placed in PC1 for higher resolution and was completely contained in the field of view. However, the outer annulus of the cluster to the north is missing. Because of the possibility for mass segregation between the core and the outer part of the cluster due to different mass stars forming preferentially in different parts of the cluster, we have corrected for the missing outer region, and in fact the brightest stars are found primarily in the PC image. We have corrected for the missing outer region by multiplying the star counts in WF2 + WF3 + WF4 by 1.8, the estimate of the missing spatial area assuming a symmetrical cluster. In deriving the IMF we have eliminated stars located far from the main sequence on the color-magnitude diagram; that is, residual red giant branch stars.

As in our previous studies, we have made no correction for the presence of binary star systems in the cluster since this effect is unknown at this time. However, we have estimated the potential effect on the IMF by assuming that half of all stars in each mass bin are binaries of equal luminosity and hence mass. In this case the IMF steepens by 3.5 σ. Without information about the frequency and mass ratios

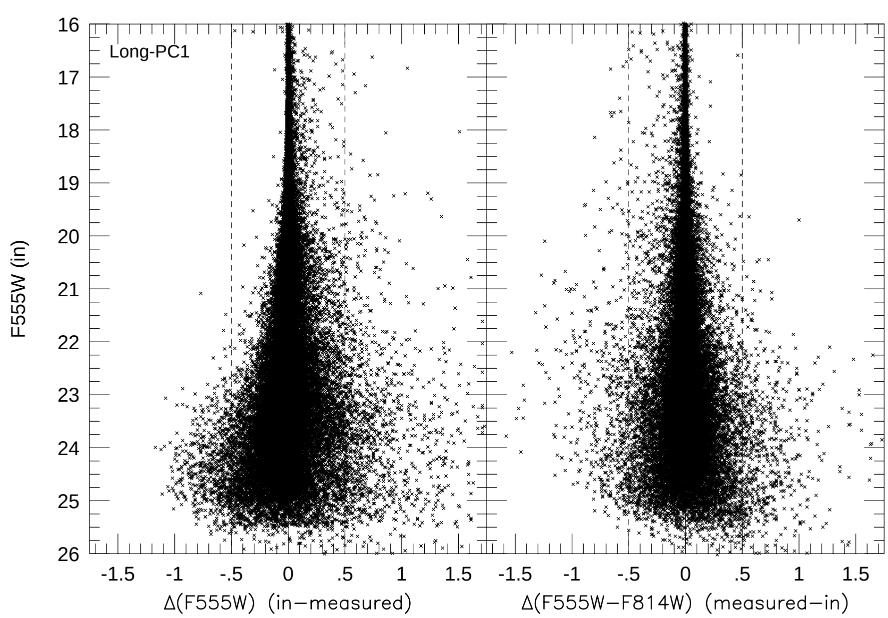

FIG. 7.—Measuring errors for the fake stars that were added to the long exposure F555W PC1 image. On the left is the error in the magnitude, and on the right is the error in the F555W–F814W color for the 48,000 fake stars that were recovered.

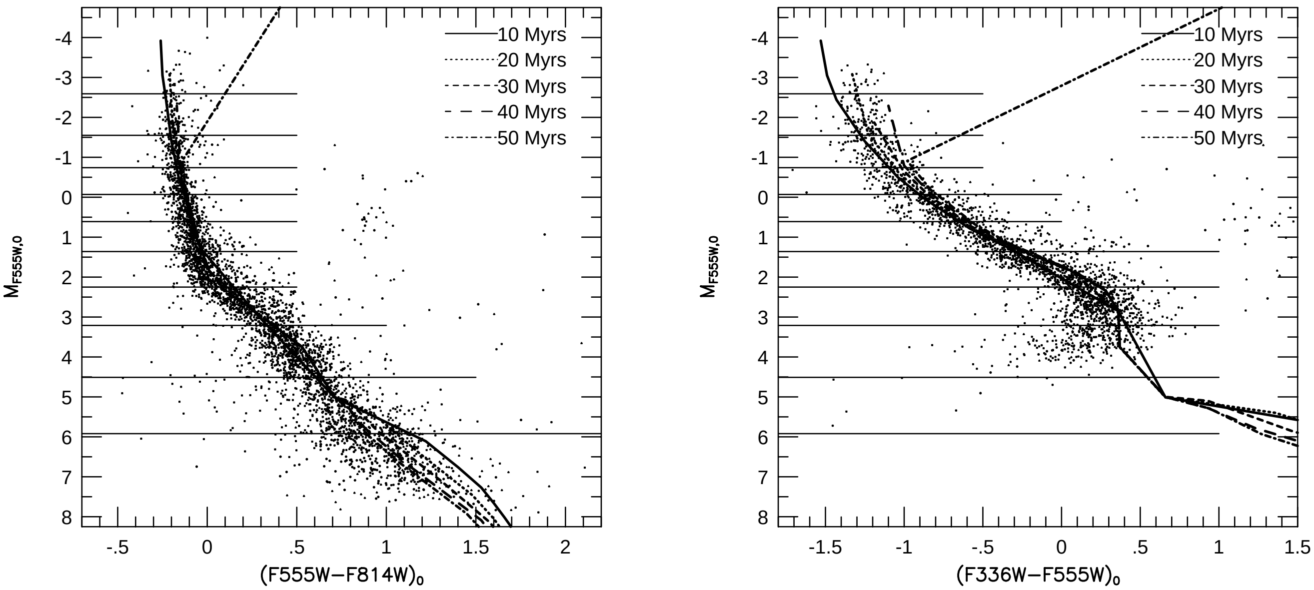

FIG. 8*a* FIG. 8*b*

FIG. 8.—Color-magnitude diagrams for (*a*) $(F555W-F814W)_0$ and (*b*) $(F336W-F555W)_0$ are shown after correcting the photometry for reddening and statistically removing a background field contribution. Isochrones, as described in the text, for ages 10–50 Myr, are superposed. The data are shown as tiny points so that the isochrones will be more visible. The partial horizontal lines denote the magnitudes that correspond to the mass bins used in determining the IMF.

of binaries for different mass ranges we cannot make a proper correction, but this does give some idea of what effect the presence of binaries might have on derived IMFs in general.

We have computed the stellar mass function, ξ, which is the number of stars per logarithmic mass interval per unit area, in nine mass bins spanning the main sequence in our color-magnitude diagram. We chose the mass bins to be approximately equal in ratio, and they run from 9 $M_\odot$ ($M_{F555W} = -2.6$) down to 0.85 $M_\odot$ ($M_{F555W} = 5.9$). Beyond this lower mass limit, the incompleteness factors rise quickly, and we do not feel confident in pushing lower (see Fig. 6). The magnitude bins that correspond to the mass bins are indicated on the color-magnitude diagrams in Figure 8.

The mass function that we compute is shown in Figure 9 and listed in Table 4. The slope Γ [$= d(\log \xi)/d(\log M)$] of this well-behaved mass function is -1.23 ± 0.08 for stars 0.85–9 $M_\odot$. The uncertainty in the slope is the uncertainty in fitting a line through all of the mass bins and is a measure of how well the mass bins agree with each other. This slope is to be compared to a Salpeter (1955) slope of -1.35. Will et al. (1995) had computed the IMF from ground-based data for stars 2–8 $M_\odot$, and obtained a slope of -1.1 ± 0.3. The larger uncertainty of the Wills et al. slope is presumably a reflection of the difficulties of doing photometry from crowded ground-based images. Their slope and ours agree well within the uncertainties, but we have now pushed the mass range to a significantly lower stellar mass and have resolved the stars in the center of the cluster.

As a test of the robustness of this IMF, we have computed the IMF under two plausible variations on our underlying assumptions. First, if we had used a 30 or 40 Myr isochrone, the IMF slope becomes -1.0 ± 0.2. Thus,

TABLE 4

THE INITIAL MASS FUNCTION

Mass ($M_\odot$)	$\log \xi$ (Number/log M/pc^2)	$\sigma_{\log \xi}$	Γ	σ_Γ
6.9–9.0	−0.19	0.06	−1.23	0.08
5.3–6.9	−0.05	0.05		
4.1–5.3	0.01	0.05		
3.2–4.1	0.23	0.04		
2.4–3.2	0.30	0.03		
1.8–2.4	0.57	0.02		
1.4–1.8	0.68	0.02		
1.1–1.4	0.88	0.02		
0.85–1.1	0.82	0.02		

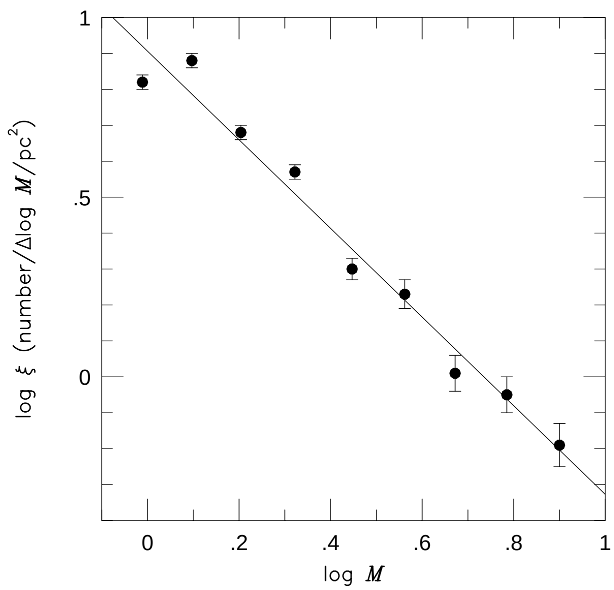

FIG. 9.—Cluster IMF, the logarithm of the stellar mass vs. the logarithm of the number of stars divided by the stellar logarithmic mass interval and the area. The error bars are computed from the uncertainties in the number of stars counted and in the incompleteness correction factors. The solid line is a least-squares fit to the nine mass bins.

the slopes determined assuming these longer ages are only different from that determined for our chosen age by about 1 σ. Second, if we had not used the adjustment to the isochrones settled on for the R136 analysis (Hunter et al. 1995) but had instead ascribed the entire F555W–F814W offset of the isochrones to reddening in the cluster, the reddening we would have used would have been an $E(B-V) = 0.1$. For this choice of reddening, the slope of the IMF would be -1.2 ± 0.06, less than 1/2 σ different. Thus, we conclude that our determination of the slope of the cluster IMF is fairly robust.

We have also measured the IMF slopes separately for the core of the cluster, defined to be the PC field of view, and the outer regions of the cluster, defined to be the WF fields of view. For the mass range 0.85–9 $M_\odot$, the slope of the IMF in the core of the cluster is indistinguishable from that in the outer regions. The slope in the core is -1.21 ± 0.10, while that in the outer region is -1.25 ± 0.08. The cluster core does contain brighter stars that are not included in our IMF because they are saturated in our images, and these brightest stars are not as common in the outer regions of the cluster, but for the mass range 0.85–9 $M_\odot$ there is no distinction between the core and the outer region.

Inspection of Figure 1 shows that there is a clustering of bright stars along the bottom (western) edge of WF4, about 21 pc from the center of NGC 1818. This group of stars stands out from the main body of the cluster itself because of the concentration of bright stars in a region otherwise populated by fainter stars. The appearance is that of a star forming event that was separate from NGC 1818, either entirely physically separated from that which formed NGC 1818 or perhaps a separate event within the same natal cloud. The field star-subtracted color-magnitude diagram of this subcluster is shown in Figure 10. A comparison of the color-magnitude diagrams of the subcluster with that of the rest of the cluster shows that they are in fact very similar, which suggests that their ages are also similar. Thus, it is plausible that the subcluster and the main cluster were formed as part of the same star forming event, perhaps even within the same gas cloud complex. The subcluster, defined to be 6.17×5.76 pc in size, has too few stars to reliably determine a separate IMF for it. However, if we subtract the subcluster stars from the cluster as a whole in determining the IMF, the slope of the cluster IMF does not change.

6. IS THE INITIAL MASS FUNCTION A UNIVERSAL FUNCTION?

Determining an IMF from a color-magnitude diagram is a laborious affair. For that reason, it has taken many years for measurements of the IMF to accumulate to the point where one can begin to see if the IMF varies with different object type or galactic environment. But, now, with measurements of the IMF in some 42 stellar clusters and associations in the Milky Way, Magellanic Clouds, M31, and M33, as well as several determinations for field stars in a subset of these galaxies, we can examine this question. Hunter (1995) has tabulated some IMF slopes and their appropriate stellar mass ranges for studies that have determined the IMF from color-magnitude diagrams, and, for massive stars, from spectral classifications. These include only Local Group galaxies since stellar counts and spectral classifications are observationally difficult beyond our galactic neighborhood.

The cluster and OB association studies include NGC 346 in the SMC (Massey et al. 1995b), the 30 Doradus region in the LMC (Parker & Garmany 1993), the luminous cluster R136 (Hunter et al. 1996c), four LMC OB associations (Massey et al. 1995b), NGC 2004 in the LMC (Bencivenni et al. 1991), the average of five young LMC clusters (Sagar & Richtler 1991), the average of six old LMC clusters (Mateo 1988), the average of 12 Milky Way OB associations (Massey et al. 1995a), eight Milky Way open clusters (Phelps & Janes 1993), the giant OB association NGC 206 in M31 (Hunter et al. 1996b), and the giant H II region NGC 604 in M33 (Hunter et al. 1996a). The IMFs in these studies have been determined for different stellar mass ranges, some for only stars more massive than 25 $M_\odot$, others for intermediate-mass stars, but none extend to stars less

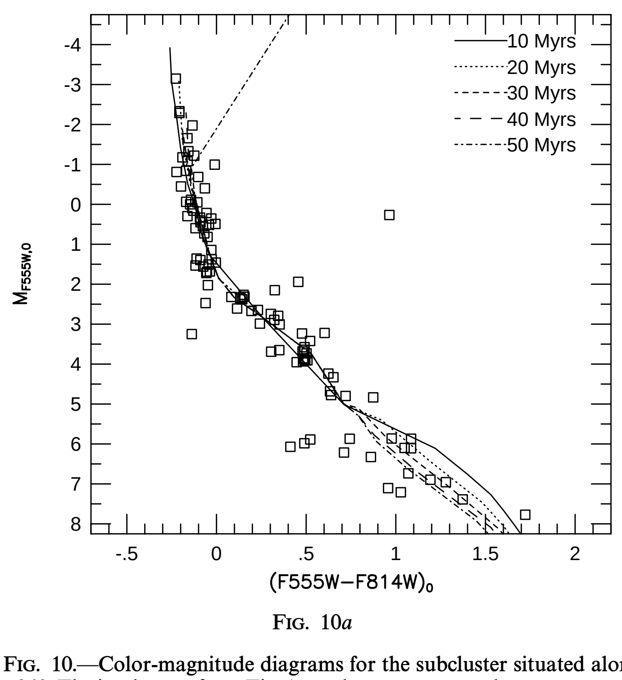

FIG. 10*a*

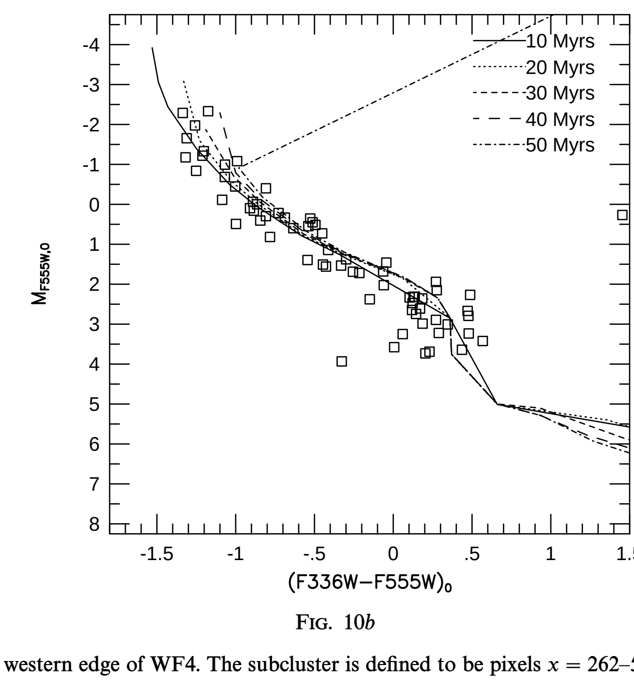

FIG. 10*b*

FIG. 10.—Color-magnitude diagrams for the subcluster situated along the western edge of WF4. The subcluster is defined to be pixels $x = 262$–519 and $y \leq 240$. The isochrones from Fig. 1 are shown superposed.

massive than 0.85 $M_\odot$. Massey et al. (1995b) also discuss the IMFs of massive field stars in the SMC, LMC, and Milky Way, and Hunter & Massey (1990) calculate the collective IMF for the most massive stars in a large sample of small Galactic H II regions. The clusters, OB associations, and massive field stars are all relatively young objects.

The slopes of the IMFs measured in these studies are shown in Figure 11. Among the stellar associations and clusters, no statistically significant variation can be seen among the five galaxies that are represented. Regrettably, the uncertainties are usually fairly high, particularly in M31 and M33. However, with the exception of the study of old clusters in the LMC by Mateo (1988) the slopes appear to be the same within the uncertainties. Furthermore, the slopes cluster around the original Salpeter (1955) IMF slope (1.35). Two clusters in Mateo's study have been observed by others who determined shallower slopes that are close to the Salpeter value (1.2 and 1.3 instead of ≤ 2.4 and 2.0; Cayrel et al. 1988; Chiosi et al. 1989). According to Mateo (1993), the most probable reason for the differences in IMF slopes between his study and those of others is due to differences in philosophy of incompleteness corrections. Thus, it is doubtful that the clusters observed by Mateo are actually different from the other clusters discussed here.

It is interesting that although the objects in these studies are clusters or associations, that is, moderately large star forming events, they do span a range in richness and spatial concentrations of the stars (Hunter 1995; Hunter et al. 1996b). R136, for example, has the highest concentration of stars, 100–300 times more concentrated than a typical OB association, and is very rich in massive stars. In fact, it has the mass and concentration of a small Milky Way globular cluster (Hunter et al. 1995). Yet, even this extreme star formation event has produced intermediate-mass stars with

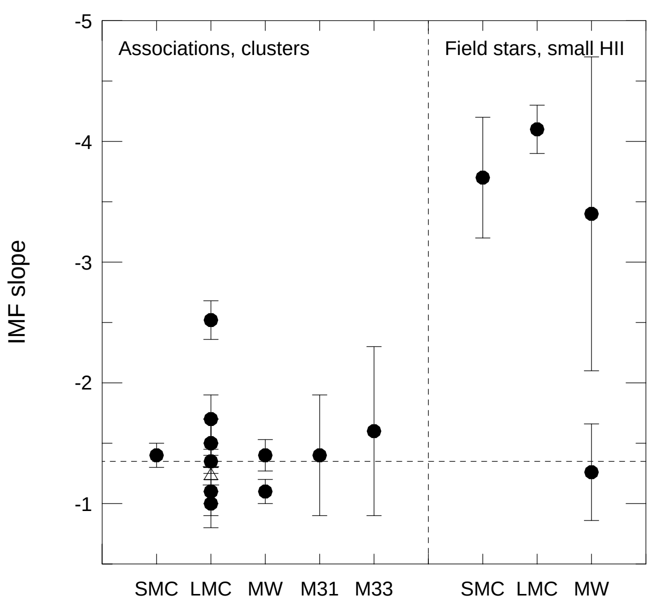

FIG. 11.—Some IMF slopes measured in Local Group galaxies, based on color-magnitude diagrams and, for high-mass stars, from spectral classifications. The dashed line is the Salpeter (1955) IMF slope of -1.35. The slopes are divided into those determined for large stellar aggregates, stellar clusters and associations, and those determined for field stars or small Galactic H II regions containing only a few massive stars. See the text for references and Hunter (1995) for a tabulation of the IMFs and the stellar mass ranges for which they were determined. The value for NGC 1818 determined here is represented as an open triangle.

the same proportions seen in less extreme events. NGC 604, a giant H II region in M33, by contrast contains comparable numbers of luminous stars as R136 but these stars are spatially concentrated like those in a typical OB association. NGC 604 too has a "normal" IMF. NGC 206, the giant OB association in M31 also contains hundreds of luminous stars but they are more sparsely distributed than those in NGC 604, and yet NGC 206 also has a comparable IMF. Finally, regular OB associations in the Milky Way and Magellanic Clouds are less rich, containing only 10–100 OB stars, but they too have a Salpeter-like IMF.

In addition to not seeing any trend in the IMF slope with richness or spatial concentration of the stars in a cluster, no trend is seen among galaxies despite differences in galactic environments, including metallicity, presence of spiral arms, and amount of interstellar shear. Finally, we note that the IMF slopes are independent of the mass range covered here, that is, massive stars are similar to intermediate-mass stars. Therefore, within the range of characteristics sampled by the Local Group galaxies and radially within these galaxies, the stellar IMF of young clusters and associations appears to be invariant.

However, this particular value of the IMF slope may not extend to all sizes of star forming events. Massive field stars were presumably formed in small star forming events containing only one or a few massive stars, and Massey et al. (1995b) have found that the massive field stars of the SMC, LMC, and Milky Way all have similar IMFs but that this IMF slope is significantly steeper than those found for clusters and associations. In a comparison of various studies in the literature, Scalo (1986) also points out that cluster IMFs are generally flatter than field star IMFs for massive stars ($>10\ M_\odot$). Hunter & Massey (1990) identified the most massive star in each H II region in a sample of small Galactic molecular clouds, H II regions that were ionized by only one or a few massive stars. Thus, these star forming events are probably closer in scale to those that produced the field massive stars than to those that produced the OB associations discussed above. They found that the IMF of this ensemble of stars from different regions had a Salpeter slope, like those of the clusters and unlike those of the field stars. The reason for the discrepancy between the small Galactic H II regions and the field stars is not clear, but the Hunter & Massey study restricted itself to the most massive star in each region rather than including the entire stellar population in the star forming region.

Although the Salpeter (1955) IMF was determined from field stars in the solar neighborhood, it was determined only for intermediate and lower mass stars ($M_V \geq -4$) rather than massive stars and so the birthplaces of these longer lived stars (whether in very small star forming events or in associations) are not known. Scalo (1986) concludes that there is observational evidence for differences between clusters and field stars only for massive stars. In agreement with this is the study of field stars in the LMC for stellar masses 0.6–1.1 $M_\odot$ by Holtzman et al. (1997). The IMF for these stars is a difficult entanglement of metallicity and star formation history, but Holtzman et al. place the slope of the IMF for these low-mass stars between -1.0 and -2.1, closer even at the extremes to the Salpeter slope than to that obtained by Massey et al. for massive field stars. Thus, studies of field stars do suggest that the massive star products of the small star forming events are not the same as those in the larger events. However, the IMF nevertheless still appears to be the same for the small star forming event in different galaxies and, hence, different galactic environments (Massey et al. 1995b).

We conclude: *For young stellar clusters and associations the IMF is independent of the spatial concentration of the stars formed, the richness of stars formed, galactic characteristics including metallicity, and, at least down to* 0.85 $M_{\odot}$, *the stellar mass range.* There appears to be some difference between the relative numbers of massive stars formed in tiny star forming events and those formed in larger OB associations and clusters, but for a given type of event the star formation process seems to be independent of the galactic properties sampled by the Local Group galaxies. *In other words, the star formation process is truly local, and once a cloud begins forming stars, it does so independently of the galaxy in which it is located.*

7. INTEGRATED PROPERTIES OF NGC 1818 AS A STAR CLUSTER

NGC 1818 is one of the intriguing " populous clusters " of the LMC. Just what are the integrated properties of this cluster and how do they compare to other star clusters? We have summed the mass in stars from 0.85 to 9 $M_{\odot}$ and found the total to be 9040 $M_{\odot}$. If the IMF that we measured extends up to 100 $M_{\odot}$ and down to 0.1 $M_{\odot}$, then the total mass in stars is 2.8×10^4 $M_{\odot}$. This is about half the mass estimated by Hunter et al. (1995) for R136, the compact, luminous star cluster in 30 Doradus. Globular clusters in the Milky Way have masses of order 10^5 to 10^6 $M_{\odot}$. So, R136 is at the low end of the mass range of globular clusters, and NGC 1818 is smaller still.

To estimate the luminosity of the cluster, we have assumed an $(\mathrm{F555W–F814W})_0$ color of 0.5 for stars without F555W measurements. We also compensated for the bright stars that were saturated on the short F555W image by assuming an F555W magnitude of 13.5 for each star. The total absolute F555W magnitude of NGC 1818 estimated in this way today is -9.3. The radius that contains half the light, $R_{0.5}$, is 3.2 pc, and the observed surface brightness within the half light radius $\Sigma_{0.5}$ is 7100 $L_{V,\odot}$ pc^{-2}. From cluster evolution models by Bruzual (1993), we would expect NGC 1818 to have been 1.2 mag brighter in V at an age of 4 Myr if it is now 20 Myr old. Thus, compared to R136, which is currently about 4 Myr old, NGC 1818 would have had a total magnitude of -10.5 compared to R136's -11.1 and a surface brightness $\Sigma_{0.5}$ that was about one-sixth that of R136's at the same age. The half-light radius $R_{0.5}$ is also about twice that of R136's.

So, NGC 1818 is less luminous, less compact, and less massive than R136 by factors of several. This still leaves a respectable cluster, but it is not among the more extreme star-forming events including super star clusters where $\Sigma_{0.5}$ can be several hundred times higher for objects of the same age (O'Connell, Gallagher, & Hunter 1994; Hunter, O'Connell, & Gallagher 1994). These properties seem to place NGC 1818 intermediate between open clusters and globular clusters in terms of the scale of the star-forming event.

Support for this work was provided by NASA through grant number NAS5-25421 to the WFPC1 Instrument Definition Team.

REFERENCES

Bencivenni, D., Brocato, E., Buonanno, R., & Castellani, V. 1991, AJ, 102, 137
Bruzual, A. G. 1993, private communication
Burstein, D., & Heiles, C. 1984, ApJS, 54, 33
Campbell, B., et al. 1992, AJ, 104, 1721
Cardelli, J. A., Clayton, G. C., & Mathis, J. S. 1989, ApJ, 345, 245
Cassatella, A., Barbero, J., & Geyer, E. H. 1987, ApJS, 64, 83
Cayrel, R., Tarrab, I., & Richtler, T. 1988, ESO Messenger, 54, 29
Chiosi, C., Bertelli, G., Meylan, G., & Ortolani, S. 1989, A&A, 219, 167
Davis, L. E. 1994, A Reference Guide to the IRAF/DAOPHOT Package (NOAO Publ.)
Elson, R. A. W., & Fall, S. M. 1988, AJ, 96, 1383
Gascoigne, S. C. B., & Kron, G. E. 1952, PASP, 64, 196
Hillenbrand, L. A., Massey, P., Strom, S. E., & Merrill, K. M. 1993, AJ, 106, 1906
Hodge, P. W. 1961, ApJ, 133, 413
———. 1967, Large Magellanic Cloud (Washington: Smithsonian Press)
———. 1983, ApJ, 264, 470
Holtzman, J., Burrows, C. J., Casertano, S., Hester, J. J., Trauger, J. T., Watson, A. M., & Worthey, G. 1995, PASP, 107, 1065
Holtzman, J., et al. 1997, in preparation
Hunter, D. A. 1995, Rev. Mex. A&A, 3, 1
Hunter, D. A., Baum, W. A., O'Neil, E. J., & Lynds, R. 1996a, ApJ, 456, 174
———. 1996b, ApJ, 468, 633
Hunter, D. A., & Massey, P. 1990, AJ, 99, 846
Hunter, D. A., O'Connell, R. W., & Gallagher, J. S. 1994, AJ, 108, 84
Hunter, D. A., O'Neil, E. J., Lynds, R., Shaya, E., & Groth, E. J. 1996c, ApJ, 459, L27
Hunter, D. A., Shaya, E. J., Holtzman, J. A., Light, R. M., O'Neil, E. J., & Lynds, R. 1995, ApJ, 448, 179
Hunter, D. A., & Thronson, H. A. 1995, ApJ, 452, 238
Kurucz, R. 1993, ATLAS9 Stellar Atmospheres on CD-ROM, (Cambridge: Smithsonian Astrophys. Obs)
Massey, P., Johnson, K., & Degioia-Eastwood, K. 1995a, ApJ, 454, 151
Massey, P., Lang, C. C., Degioia-Eastwood, K., & Garmany, C. D. 1995b, ApJ, 438, 188
Mateo, M. 1988, ApJ, 331, 261
———. 1993, in ASP Conf. Ser. 48, The Globular Cluster–Galaxy Connection. Globular Clusters within the Context of their Parent Galaxies, ed. G. H. Smith & J. P. Brodie (San Francisco: ASP), 387
Meurer, G. R., Cacciari, C., & Freeman, K. C. 1990, AJ, 99, 1124
O'Connell, R. W., Gallagher, J. S., & Hunter, D. A. 1994, ApJ, 433, 65
Panagia, N., Gilmozzi, R., Machetto, F., Adorf, H.-M., & Kirshner, R. P. 1991, ApJ, 380, L23
Parker, J. W., & Garmany, C. D. 1993, AJ, 106, 1471
Phelps, R. L., & Janes, K. A. 1993, AJ, 106, 1870
Robertson, J. W. 1974, A&AS, 15, 261
Sagar, R., & Richtler, T. 1991, A&A, 250, 324
Salpeter, E. E. 1955, ApJ, 121, 161
Scalo, J. M. 1986, Fund Cosmic Phys., 11, 1
Schaerer, D., Meynet, G., Maeder, A., & Schaller, G. 1993, A&AS, 98, 523
Searle, L., Wilkinson, A., & Bagnuolo, W. G. 1980, ApJ, 239, 803
Stahler, S. W. 1983, ApJ, 274, 822
Stetson, P. B. 1987, PASP, 99, 191
van den Bergh, S. 1981, A&AS, 46, 79
Will, J.-M., Bomans, D. J., & de Boer, K. S. 1995, A&A, 295, 54
Woolley, R. v. d. R. 1960, MNRAS, 120, 214

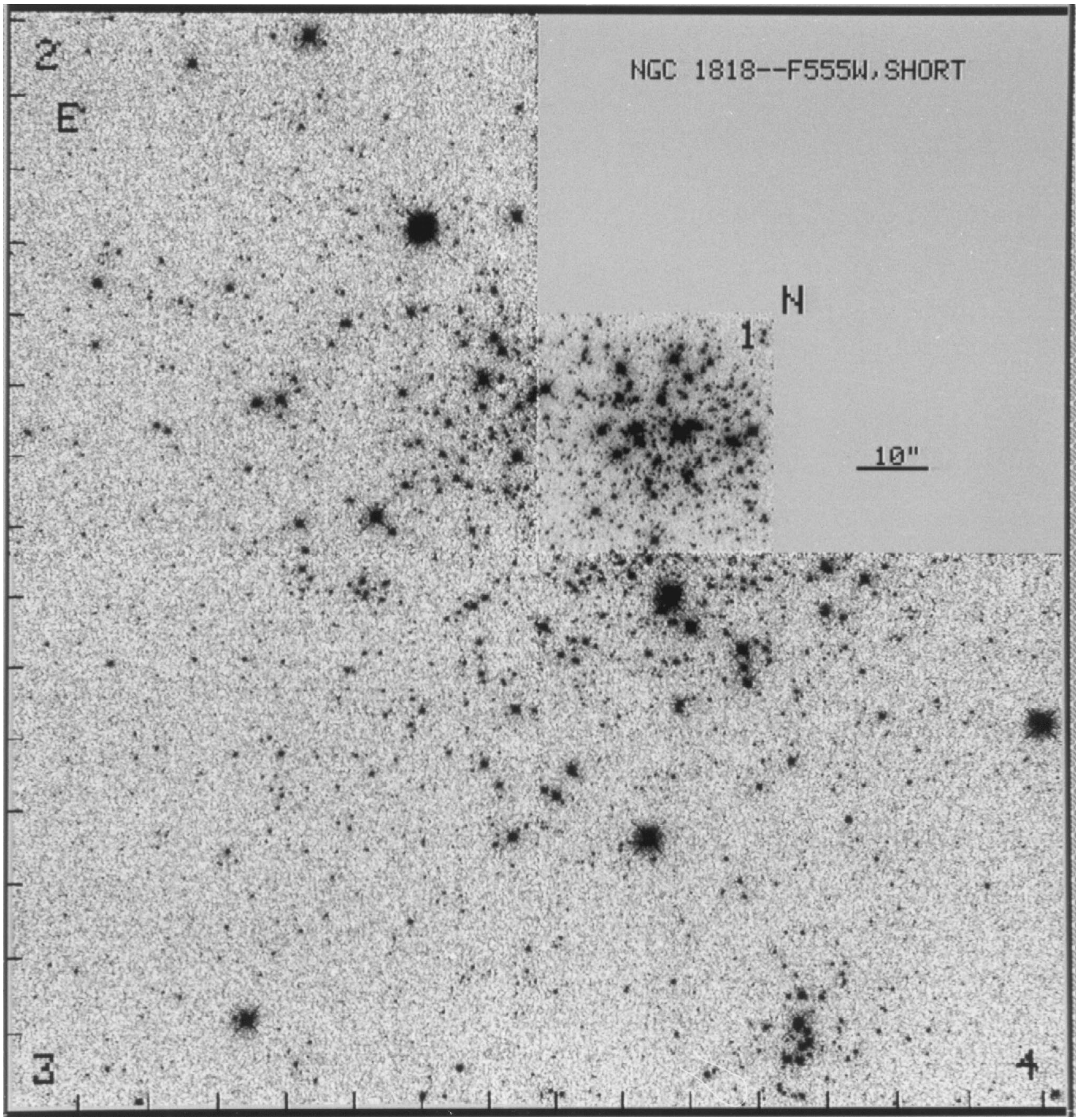

FIG. 1*a*

FIG. 1.—Short-exposure F555W images of the NGC 1818 field are shown. (*a*) Mosaic of the four CCD areas. Each CCD is identified with a number in a corner of the mosaic. The ticks along the left and bottom sides mark every 100th pixel beginning with pixel 100. The PC chip has been scaled to the same pixel size as the WF chips. North is 44°.7 clockwise from up, and north and east are marked as "N" and "E." (*b*) PC1 image is shown alone for better clarity of the center of the cluster.

HUNTER et al. (see 478, 125)

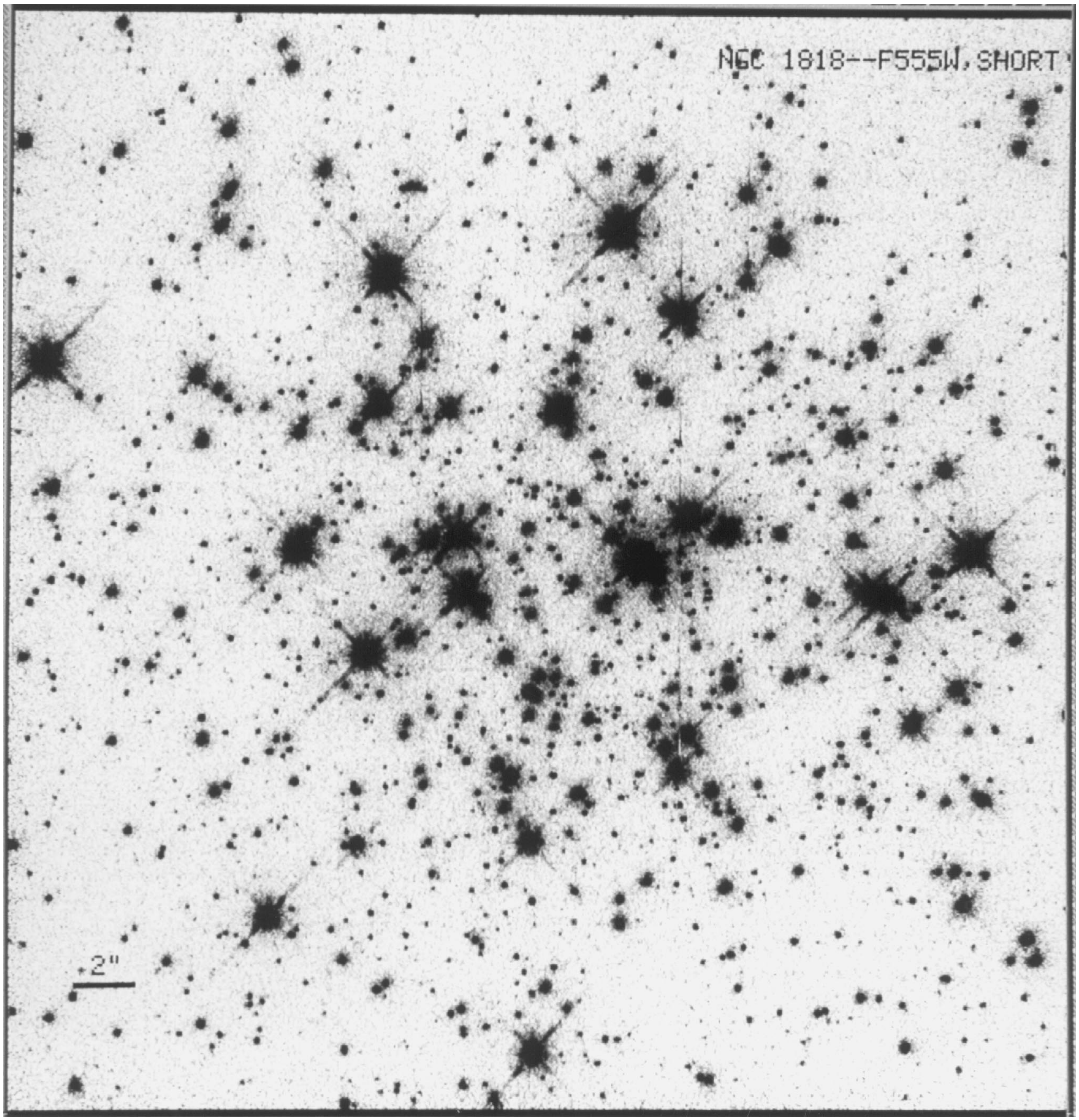

FIG. 1*b*

HUNTER et al. (see 478, 125)